Lapuebla-Ferri, A.; Perez Del Palomar, A.; Herrero, J.; Jimenez Mocholi, AJ. (2011). A patient-specific FE-based methodology to simulate prosthesis insertion during an augmentation mammoplasty. Medical Engineering & Physics. 33(9):1094-1102. doi:10.1016/j.medengphy.2011.04.014

A patient-specific FE-based methodology to simulate prosthesis insertion during an augmentation mammoplasty

Andrés Lapuebla-Ferri[a], Amaya Pérez del Palomar[b], Javier Herrero[c] and Antonio-José Jiménez-Mocholí[a]

[a]*Department of Continuum Mechanics and Theory of Structures.*
Universitat Politècnica de València.
Camino de Vera. E-46022 Valencia (Spain).
Phone: (+34) 963 87 76 74. Fax: (+34) 963 87 96 79.

[b]*Department of Mechanical Engineering.*
Aragón Institute of Engineering Research (I3A). University of Zaragoza.
María de Luna, 3. E-50018 Zaragoza (Spain).
Phone: (+34) 976 76 19 12. Fax: (+34) 976 76 25 78

[c]*Alma IT Systems.*
Carolinas 22, E-08012 Barcelona (Spain).
Phone: (+34) 932 380 952.

Comments to the author:

Andrés Lapuebla-Ferri. anlafer0@mes.upv.es

Department of Continuum Mechanics and Theory of Structures. School of Industrial Engineering. Universitat Politècnica de València. Camino de Vera. E-46022 Valencia (Spain).

Phone: (+34) 963 87 76 74. Fax: (+34) 963 87 96 79.

Abstract

Breast augmentation surgery is a widespread practice for aesthetic purposes. Current techniques, however, are not able to reliably predict the desired final aspect of the breast after the intervention, whose success relies almost completely on the surgeon's skill. In this way, patient-specific methodologies capable of predicting the outcomes of such interventions are of particular interest. In this paper, a finite element biomechanical model of the breast of a female patient before an augmentation mammoplasty was generated using computer tomography images. Prosthesis insertion during surgery was simulated using the theory of finite elasticity. Hyperelastic constitutive models were considered for breast tissues and silicone implants. The deformed geometry obtained from finite element analysis was compared qualitatively and quantitatively with the real breast shape of the patient lying in supine position, with root-mean-squared errors less than 3 mm. The results indicate that the presented methodology is able to reasonably predict the aspect of the breast in an intermediate step of augmentation mammoplasty, and reveal the potential capabilities of finite element simulations for visualization and prediction purposes. However, further work is required before this methodology can be helpful in aesthetic surgery planning.

Key terms

Breast augmentation; breast biomechanics; finite element method, hyperelastic behavior, surgery planning.

1. Introduction

Statistics from the American Society of Plastic Surgeons (1) show that about 300,000 augmentation mammoplasties took place in USA during 2009, a figure that reflects its great popularity. This cosmetic surgery consists of enlarging and reshaping the breasts by placing implants, which consist of an elastomeric covering containing a substance that provides the desired consistency to the breast. Exogenous biomaterials for augmentation mammoplasties have been used increasingly since the early 1960's in parallel with the demand for more and more satisfactory outcomes (2).

Prior to surgery, the clinician must collect the necessary information about the desired final aspect of the patient's breast, usually via anthropometric studies, and the clinical information of the patient which is needed to perform the intervention according to current protocols. In this way, a pre-surgery planning is developed, that includes the location, type, size and shape of the implants.

Human breast is a heterogeneous organ that is composed of soft tissues (fat, gland and skin) whose proportions and properties vary among individuals according to factors such as age or pregnancy. Its main function is to provide support for lactation, and not to be a load-bearing unit in the physiological situation. Additionally, as it rests on a mobile myofascial unit over the rib cage, the breast is highly deformable under the forces applied during surgery. In the present days, breast surgery outcomes can be predicted within certain degree of accuracy, but they mostly rely on the surgeon's skill. This has motivated the development of different techniques to help breast surgery planning, based on anthropometric measurements (3) or 3D scanning (4, 5).

Likewise Finite Element (FE) analysis is a widespread tool in the field of biomechanics that can be a suitable choice for surgery simulations, as it can not only minimize the uncertainty of the results of an augmentation mammoplasty but also gain insight of the mechanical behaviour or the tissues and be helpful in surgery planning. In the literature, FE models of female breast are mostly related to the evaluation of its high mobility in order to help in the location of suspicious masses (6), provide guidance during breast biopsies (7), simulate mammographies (8, 9, 10, 11), validate non-rigid medical registration algorithms (12) or test algorithms for elastography (13). Among them, individual-specific breast models can be found. Recently, a modelling framework of a generic FE breast model customized to an individual that was simulated under gravity load was developed to predict the final breast shape (14). Similarly (15), a patient-specific FE model of a hyperthropic breast was simulated in lying and standing-up positions, mapping spatial features in the model to manual landmarks plotted in patient's skin. However, FE models for augmentation mammoplasties are scarce. Roose et al (16, 17) simulated a breast implant placement, and the discrepancies between FE model and the real case were attributed to the presence of biological effects unconsidered in the FE model.

This work describes a methodology to simulate the insertion of prostheses in augmentation mammoplasty through a FE model, based on medical images taken from a patient in a real clinical case. Simulations were performed in order to predict the final shape of the patient's breasts at an intermediate stage of the surgical procedure, i. e., when the prostheses are placed and the patient is still lying in supine position.

2. Materials and methods

For the present study, a clinical case of an augmentation mammoplasty in a 36-year-old European female with no anatomical abnormalities was chosen, from whom a written informed consent was obtained. Surgery in the real case was performed by placing two 365 cc silicone-filled implants in sub-glandular position, and this was reproduced with the virtual FE planning model proposed in this work.

2.1. FE model generation

A FE model of the breast was constructed from computer tomography (CT) images of the patient before augmentation mammoplasty. The images were acquired by means of Philips/Mx8000 IDT 16 CT scanner with a 512 x 512 pixel resolution in-plane; pixel size 0.8 x 0.8 mm in-plane and 0.5-mm slice thickness, with the patient lying in supine position (Figure 1a). The images were saved in DICOM format and loaded into the MIMICS 10.01 software (18), where tissues densities (defined in Hounsfield units) were computed from gray-scaled pixels. In order to perform tissue segmentation, the software automatically applied threshold values to separate fat, gland, bone and skin. As thresholding was not enough, manual segmentation was needed to better define the boundaries between tissues (Figure 1b). As gland and muscle have similar densities, they were not segmented automatically, but rather manually according to the shape of the pectoral muscle. A 3D geometric model was obtained (Figure 1c), which included fat, gland and skin. Fat and gland were considered as a homogeneous tissue for the simulation of the FE model, as reported in previous works (15, 16, 19).

The geometric model of the patient before surgery was exported to MSC.PATRAN 2006r1 (20) in order to generate the FE model (Figure 1d). A semi-automated meshing technique was applied to obtain a mesh composed of 19584 linear hexahedral elements and 25088 nodes representing the breast. The mesh was fine enough to fit the breast geometry and minimize numerical errors during analysis, considering that hexahedral elements have better convergence than tetrahedral elements (9). Subsequently, a mesh convergence test was performed, and the suitability of the chosen mesh size was checked. The skin was modelled with 5040 linear quadrilateral elements coating the periphery of the hexahedral mesh.

A second set of CT images was obtained with the same scanning device and following the same protocol as before, from the patient after surgery also lying in supine position (Figure 2a). The time elapsed between the two CT acquisitions ensured that post-surgery effects had passed and the total radiation dose received by the patient was within acceptable levels as prescribed by legislation. Like in the geometric model of the patient before surgery, a new 3D geometric model of the enlarged breast was generated (Figures 2b, 2c). This model was kept for further comparison by superposition with the deformed breast shape provided by the FE model analysis. For this purpose, geometric locations of the outer surface of the chest wall were recorded in both geometric models.

2.2. Constitutive modelling

As the tissues of the breast, like most soft biological tissues, are anisotropic, inhomogeneous and undergo large deformations with negligible volume change, finite elasticity was used for the constitutive modelling of the different tissues involved.

Isotropy was assumed for the breast since fatty and glandular tissues have not a preferential fiber direction. A strain-energy density function **Ψ** in terms of the strain invariants was introduced to characterize quasi-incompressible, near isotropic hyperelastic materials, such as the breast tissues. According to the kinematic assumption, **Ψ** was written in the decoupled form (21) as:

$$\psi(C) = \psi_{vol}(J) + \psi_{iso}(C^s) = \frac{1}{D} + C_1(I_1 - 3) \qquad [1]$$

where $\psi_{vol}(J)$ and $\psi_{iso}(C^s)$ are given scalar-valued functions of $J = \det F$ and $C^s = J^{2/3}F^TF$, which describe the volumetric (dilatational) and the isochoric (distortional) responses of the material, respectively, $\mathbf{C^s}$ being the right Cauchy-Green tensor and **F** the deformation gradient. The simplest hyperelastic model, the neo-Hookean model, was assumed for $\psi_{iso}(C^s)$ in expression [1], $\mathbf{I_1}$ being the first invariant of $\mathbf{C^s}$, and $\mathbf{C_1}$ a constant that is equal to half the initial shear modulus **μ** of the tissue, which takes into account the stiffness of the breast.

The value of $\mathbf{C_1}$ should be computed from experimental measurements taken on the particular tissues of the patient and their arrangement on the breast. However, in the FE model the breast was assumed to be homogeneous, and accordingly a rigorous parameterization of $\mathbf{C_1}$ was not necessary, so $\mathbf{C_1}$ values previously reported in the literature were used. Samani et al. (22) reported mean values of Young's modulus for normal breast tissues ($\mathbf{E_{fat}}$ = 3.24 kPa and $\mathbf{E_{gland}}$ = 3.25 kPa). Therefore, a Young's modulus of 3.24 kPa was considered for the homogenized breast tissue in the present work. Considering a Poisson's ratio of **υ** = 0.499 to take into account the incompressibility of the breast, as it is mainly composed of water, the final value of $\mathbf{C_1}$ for the homogenized breast tissues of the patient was 0.54 kPa.

Skin is considered an anisotropic and hyperelastic tissue (23), but in the performed simulations it was supposed to be isotropic for simplicity. Again, a hyperelastic behaviour able to withstand large deformations was supposed in the FE model with the following polynomial strain-energy density function ψ_{sk}:

$$\psi_{sk} = \sum_{i+j=1}^{N} C_{ij}(I_1 - 3)^i (I_2 - 3)^j \qquad [2]$$

Expression [2] was fitted for N=2 to the stress-strain experimental results obtained by Gambarotta et al. (24) by the least-square method, thus obtaining the following parameters: C_{10} = 31 Pa, C_{01} = 30 Pa, C_{11} = 22.5 Pa, C_{20} = 50 Pa and C_{02} = 60 Pa. The elements representing the skin in the FE model were assigned a uniform thickness of 1 mm, as reported in the literature (19).

The constitutive relationships for these tissues were implemented in ABAQUS v.6.5 (25), and the locking of hexahedral elements was avoided using a standard mixed theory.

2.3. Boundary conditions

In a FE model, a suitable definition of the boundary conditions can be more significant than the material properties in terms of accuracy of results (19). To properly simulate the mechanical response of the breast during prosthesis insertion, fixed

displacement boundary conditions were imposed to the nodes of certain locations in the FE model (Figure 3). The nodes corresponding to the thoracic wall were restricted as the underlying myofascial unit is firmly attached to the rib cage. Mid-saggital plane nodes were also restrained since the sternum does not move during surgery. Finally, top and bottom surfaces were also fixed as they limit the upper and lower parts of the breast, respectively, and they are distant enough not to alter the accuracy of results.

2.4. Simulation of prosthesis insertion

At present, augmentation mammoplasty is a straightforward procedure. The surgeon makes an incision in the armpit, in the inframammary fold or along the areolar border of the breast, and creates an internal pocket where the prosthesis is to be placed. The implant is then pushed through the incision to its placement in submuscular or subglandular position. In order to simulate this procedure using the FE model of the patient before surgery, the scheme shown in Figure 4 was followed.

Clearly, prosthesis insertion during an augmentation mammoplasty involves a displacement of the tissues and an increase in breast volume. In the FE model, empty volumes mimicking the pockets where the prostheses could be allocated were created by introducing an equivalent pressure inside each breast. The plastic surgeon that carried out the augmentation mammoplasty provided the location of the prostheses, as shown in the second set of CT images (Figure 2b). The initial configuration $\mathbf{\Omega_0}$ (Figure 4a) was supposed to be the mechanical reference state. In order to apply the pressures, an internal loading surface in the anterior part of the thoracic wall was generated for each breast (Figure 5), consisting of 1213 linear quadrilateral 0.6 mm-thick (usual in breast implant shells) membrane elements, which coincided with the faces of the hexahedral mesh representing the homogenized breast tissue. Pressure was applied on the loading surfaces (Figure 4b) until an empty volume of 365 cc (the same volume as the implant size) was obtained for each breast in a new deformed configuration $\mathbf{\Omega_1}$ (Figure 4c). The analysis was performed in ABAQUS v.6.5 (25) by means of a UMAT user-defined material subroutine which permitted to compute the associated deformation gradient $\mathbf{F_0^1}$. The values of the applied pressures were 0.25 kPa and 0.24 kPa for the left and right breasts, respectively. The small difference of 4.2 % between both values was assumed to be due to the non-symmetry of the FE model respect to the mid-saggital plane. This loading procedure was previously reported by Lanchares et al. (26).

To include the prostheses in the FE model, the deformed model configuration $\mathbf{\Omega_1}$ was exported to MSC.PATRAN 2006r1 (20) and 3639 additional linear hexahedral meshes were generated in each empty volume (Figure 6) before performing a new simulation. A neo-Hookean constitutive model was considered for these meshes, with $\mathbf{C_1}$ = 0.71 kPa, as reported in the literature data (8). The inputs applied to the modified FE model were the internal pressures and the deformation gradient $\mathbf{F_0^1}$ previously obtained. Again, the model deformed into a new configuration $\mathbf{\Omega_2}$ as the internal stresses balanced the pressure loads, and a new deformation gradient $\mathbf{F_0^2}$ was computed (Figure 4d).

3. Results

As a preliminary evaluation of the performance of the proposed methodology, the deformed shape provided by the FE model analysis was compared with the real

geometric model of the patient's breast following surgery. It has to be remarked that this should be done considering the model of the patient in a standing-up position, as it is usually done in the clinical practice to verify the outcomes of the surgical intervention. Instead of this, and due to the lack of a geometric model in such a position, comparisons were made with the patient in supine position. As described in section 2.1., locations of the outer surface of the chest wall were used to superimpose the deformed shape of the FE model over the geometric model of the patient following surgery, assuming that the ribs did not deform from the first to the second image set. Figure 7 shows this qualitative comparison, which reveals a good matching between the deformed shape of the FE model and the final aspect of the patient.

Additionally, two different procedures were proposed for the quantitative verification. The first one quantified the global difference between the deformed shape of the FE model in the deformed configuration $\mathbf{\Omega_2}$ and the geometric model of the patient after surgery, similarly to the procedure reported by Chung et al. (8). As regards the peripheral nodes $\mathbf{n_{FE}}$ in the FE model, the root-mean-square (RMS) of the projection distance between every node $\mathbf{x_{FE}}$ of the FE model and the closest location $\mathbf{x_P}$ in the geometric model of the patient after surgery was computed [3]. The RMS values for left breast, right breast and both breasts were 2.73 mm, 2.32 mm and 2.53 mm, respectively.

$$RMS = \sqrt{\frac{1}{n_{FE}} \sum_{i=1}^{n_d} \left\| x_{FE,i} - x_{P,i} \right\|^2} \qquad [3]$$

The degree of coincidence between the deformed shape of the FE model and the geometry of the patient is illustrated in Figure 8. Apart from a small group of nodes in the armpits or the breast contours, most of the nodes of the FE model were close to the real geometry of the patient following surgery. The maximum deviation found was 11 mm in the X-direction for a small group of nodes in the right breast, but this contrasts with the nodal mean deviation of 0.91 mm in the X-direction for both breasts. Roose et al. (17) tested a method to simulate an augmentation mammoplasty in four patients, obtaining a maximum error less than 9 mm with a mean error less than 4 mm. These values were found to be similar to those obtained in this work.

The second quantitative method for model verification consists of local comparisons. A set of nodal markers were chosen in the patient's geometry following surgery (Figure 9a). These points were chosen because they correspond to anatomic locations that play a key role in the outcomes of an augmentation mammoplasty, i.e. the final aspect of the breast. Also, the number and location of these markers were helpful to check the breast contours in the deformed shape of the FE model. The Euclidean distances from the markers to the equivalent nodal locations in the FE model (Figure 9b) are shown in Table 1. The RMS on the landmarks is higher than RMS values previously computed for the breast surfaces, but they are in the same order of magnitude.

4. Discussion

Human breast is an inhomogeneous structure, mainly composed of fat, gland and skin. Unlike other organs, it is not a load-bearing structure but it is capable of withstanding large deformations. Augmentation mammoplasty is a surgical technique

consisting of the insertion of prostheses inside the breasts for aesthetic purposes. In this work, the authors propose a patient-specific FE-based methodology in which the placement of the prostheses is simulated using the theory of finite elasticity. The final goal of this paper is to present a straightforward method to reliably predict the outcomes of augmentation mammoplasty. Nevertheless, some drawbacks were found and should be addressed.

The first issue deals with the prediction of the breast shape. In the present study the results refer to the patient lying in supine position due to the lack of medical images of the patient in a standing up position. Consequently, breast prediction was only partially fulfilled. However, taking into consideration that the surgeon needs to check the outcomes of the intervention while the patient is still lying in supine position, the aim of this paper is fulfilled. If a model in the standing up position was available, then also the final step of loading procedure (application of gravity loads as described in section 2.4 to the deformed configuration $\mathbf{\Omega_2}$) could have been evaluated.

Despite the fact that a detailed FE model has been built from CT images taken from the patient before surgery, some difficulties were encountered when outlining the breast contours, which can generate uncertainties for delimiting the material regions and assigning boundary conditions to the appropriate nodes in the FE model. Moreover, other structures that are thought to play a significant role in the supporting structures of the breast, such as Cooper ligaments, should be considered in further studies (27).

Fatty and glandular tissues were supposed to be uniformly arranged in the breast, and reported values of elastic moduli were used to compute parameter $\mathbf{C_1}$ in the neo-Hookean model of the breast. It was not necessary to differentiate the internal breast tissues in the context of the presented methodology, so medical images not necessarily have to be CT images. The aim of this was to find a FE model with a small number of material parameters for breast tissue characterization. Nevertheless, for an accurate customization of the FE model to a certain patient, the particular mechanical properties of the breast tissues should be computed, so further research is needed in this matter. Also, skin is known to be significantly anisotropic, but the assumption of isotropy was considered here for simplicity.

Internal processes of living tissues (growth, remodelling, etc.) expose them to *in vivo* stresses and strains (28). Also, since the initial geometry of the FE model was obtained with the patient lying in a supine, gravity-subjected position, the reference configuration used in the FE model is not completely stress-free. In addition, the surgical practice of prosthesis insertion during an augmentation mammoplasty was simulated by introducing an internal pressure in the FE model to generate a pocket. Pressure was uniformly applied, which actually is not how the surgeon performs during surgery. Nevertheless, the deformed shape of the FE model was in good agreement with the aspect of the patient following surgery, as shown by the RMS values and the Euclidean distances measured from nodal markers. While values for mammographic compressions are reported in the literature (10), to the authors' knowledge there are no reported values of applied forces during an augmentation mammoplasty, and this issue should also be properly addressed.

Finally, a deformed shape of the FE model with the meshes of the prostheses should be obtained under gravity loads, representing the patient in a standing up position, but this was not possible due to the lack of a geometric model in such position. This issue will be addressed in further works.

In spite of these geometric and material simplifications, the authors believe that the methodology and the verification methods proposed are straightforward and able to simulate prosthesis insertion in an augmentation mammoplasty. Nevertheless, further

refinements of this methodology are required, especially those related to the parameterization of the breast tissues in order to more accurately customize the patient-specific FE model, using a larger number of clinical cases. Taking into account the simplicity of this methodology, the development of further FE models for similar situations could be a valuable tool to help clinicians in breast surgery planning and in the prediction of its outcomes.

Acknowledgements

The support of Instituto de Salud Carlos III (ISCIII) through the CIBER initiative, and the support of Platform for Biological Tissue Characterization of the Centro de Investigación Biomédica en Red de Bioingeniería, Biomateriales y Nanomedicina (CIBER-BBN) are highly appreciated. The translation of this paper was funded by the Universidad Politécnica de Valencia, Spain.

References

1. American Society of Plastic Surgeons (ASPS). 2010 report of 2009 statistics: national clearinghouse of plastic surgery statistics. Report available online.

2. Van Zele, D. and Heymans, O. Breast implants: a review. Acta Chirurgica Belgica 104:158-165, 2004.

3. Qiao, Q., Zhou, G. and Ling, Y. Breast volume measurement in young Chinese women and clinical applications. Aesthetic Plastic Surgery 21:362-368, 1997.

4. Lee, H., Hong, K. and Kim, E. A. Measurement protocol of women's nude breasts using a 3D scanning technique. Applied Ergonomics 35:353-359, 2004.

5. Tepper, O. M., Small, K., Rudolph, L., Choi, M. and Karp, N. Virtual 3-dimensional modelling as a valuable adjunct to aesthetic and reconstructive breast surgery. American Journal of Surgery 192:548-551, 2006.

6. Wellman, P. S. Tactile imaging. PhD Thesis, Harvard University, 1999.

7. Azar, F. S., Metaxas, D. N. and Schnall, M. D. A deformable finite element model of the breast for predicting mechanical deformations under external perturbations. Academic Radiology 8:965-975, 2001.

8. Chung, J. H., Rajagopal, V., Nielsen, P. M. F. and Nash, M. P. A biomechanical model of mammographic compressions. Biomechanics and Modeling in Mechanobiology 7:43-52, 2008.

9. Pathmanathan, P., Gavaghan, D., Whiteley, J., Brady, M., Nash, N., Nielsen, P. and Rajagopal, V. Predicting tumour location by simulating large deformations of the

breast using a 3D finite element model and nonlinear elasticity. Lecture Notes in Computer Science 3217:217-224, 2004.

10. Ruiter, N. V., Stotzka, R., Müller, T., Gemmeke, H., Reichenbach, J. R. and Kaiser, W. A. Model-based registration of X-Ray mammograms and MR images of the female breast. IEEE Transactions on Nuclear Science 53:204-211, 2006.

11. Samani, A., Bishop, J., Yaffe, M. J. and Plewes, D. B. Biomechanical 3-D finite element modelling of the human breast using MRI data. IEEE Transactions on Medical Imaging 20:271-279, 2001.

12. Schnabel, J. A., Tanner, C., Castellano-Smith, A. D., Degenhard, A., Leach, M. O., Hose, D., Hill, D. L. G. and Hawkes, D. J. Validation of nonrigid image registration using finite-element methods: application to breast MR Images. IEEE Transactions on Medical Imaging 22:238-247, 2003.

13. Washington, C. W. and Miga, M. I. Modality independent elastography (MIE): a new approach to elasticity imaging. IEEE Transactions on Medical Imaging 23:1117-1128, 2004.

14. Rajagopal, V., Lee, A., Chung, J., Warren, R., Highnam, R. P., Nash, M. P. and Nielsen, P. M. F. Creating individual-specific biomechanical models of the breast for medical image analysis. Academic Radiology 15:1425-1436, 2008.

15. Pérez del Palomar, A., Calvo, B., Herrero, J., López, J. and Doblaré, M. A finite element model to accurately predict real deformations of the breast. Medical Engineering & Physics 30:1089-1097, 2008.

16. Roose, L., De Maerteleire, W., Mollemans, W. and Suetens, P. Validation of different soft tissue simulation methods for breast augmentation. International Congress Series 1281:485-490, 2005.

17. Roose, L., De Maerteleire, W., Mollemans, W., Maes, F. and Suetens, P. Simulation of soft-tissue deformations for breast augmentation planning. Lecture Notes in Computer Science 4072:197-205, 2006.

18. Materialise. 'MIMICS 10.01 User Documentation'. Leuven, Belgium: Materialise, 2006.

19. Tanner, C., Schnabel, J. A., Hill, D. L. G. and Hawkes, D. J. Factors influencing the accuracy of biomechanical breast models. Medical Engineering & Physics 33:1758-1769, 2006.

20. MSC Software Corporation. 'PATRAN 2006 User Documentation'. Santa Ana, CA, USA: MSC Software Corporation, 2006.

21. Holzapfel, G. A. 'Nonlinear solid mechanics'. Chichester, England: Wiley, 2000.

22. Samani, A., Zubovits, J. and Plewes, D. Elastic moduli of normal and pathological human breast tissues: an inversion-technique-based investigation of 169 samples. Physics in Medicine and Biology 52: 1565-1576, 2007.

23. Tong, P. and Fung, Y. The stress-strain relationship for the skin. Journal of Biomechanics 9:649-657, 1976.

24. Gambarotta, L., Massabò, R., Morbiducci, R., Raposio, E. and Santi, P. In vivo experimental testing and model identification of human scalp skin. Journal of Biomechanics 38:2237-2247, 2005.

25. Hibbit, Karlsson and Sorensen, Inc. 'ABAQUS User's Guide, vol. 5.8'. Pawtucket, RI, USA: HKS Inc., 1999.

26. Lanchares, E., Calvo, B., Cristóbal, J. A. and Doblaré, M. Finite element simulation of arcuates for astigmatism correction. Journal of Biomechanics 41:797-805, 2008.

27. Bakic, P. R. 'Breast tissue description and modelling in mammography'. PhD Thesis, Lehigh University, 2000.

28. Fung, Y. 'Biomechanics: mechanical properties of living tissues'. New York, USA: Springer-Verlag, 1999.

Table 1. Euclidean distances measured from the nodal markers in the FE model of the deformed shape to the equivalent locations in the geometric model of the patient following surgery. Mean = 3.36 mm. RMS = 4.05 mm.

NODAL MARKER	**EUCLIDEAN DISTANCE (mm)**
(1) Left nipple	2.99
(2) Right nipple	2.71
(3) Upper left pole	5.52
(4) Upper right pole	2.63
(5) Lower left pole	1.24
(6) Lower right pole	1.36
(7) Medial left	3.16
(8) Medial right	0.77
(9) Axilar left	5.16
(10) Axilar right	8.99
(11) Sternum	2.39

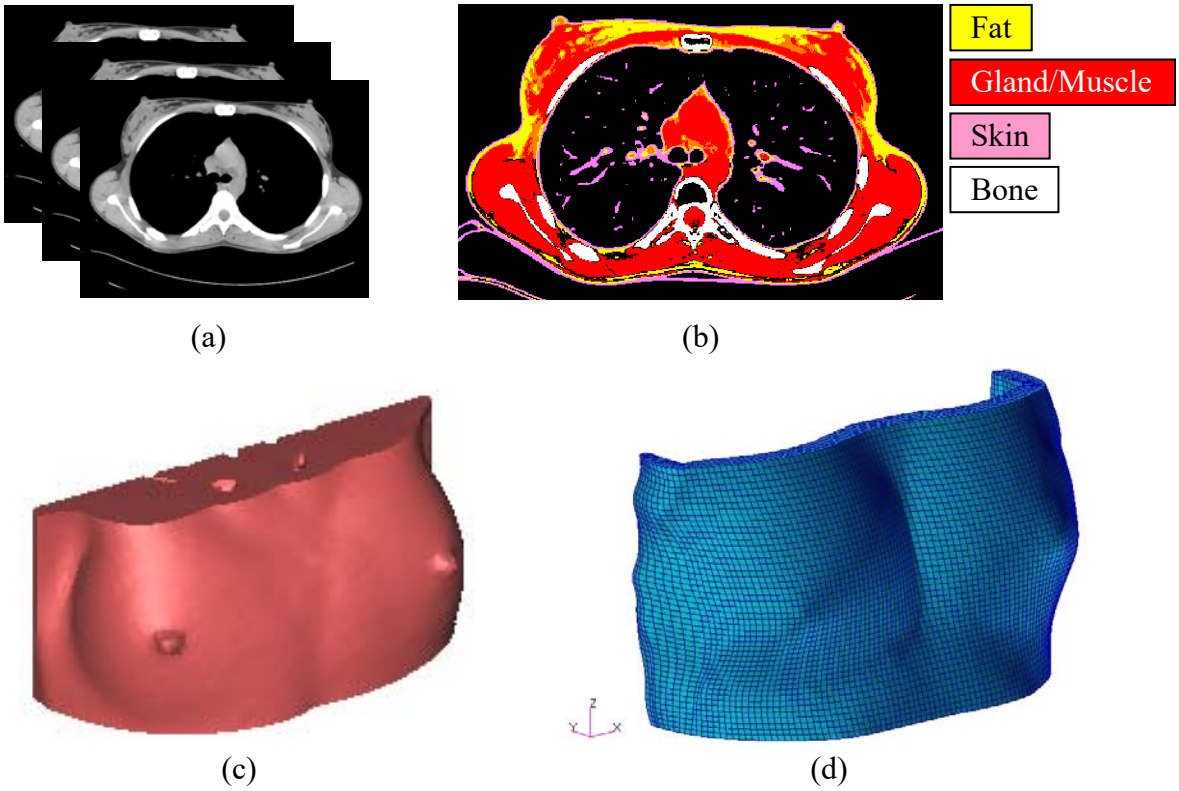

Figure 1. FE model generation of the patient's breast before augmentation mammoplasty. (a) Different CT slices taken before surgery. (b) Tissue segmentation on a slice sample. (c) Geometric model of the patient's breast. (d) Anteroposterior view of the FE mesh.

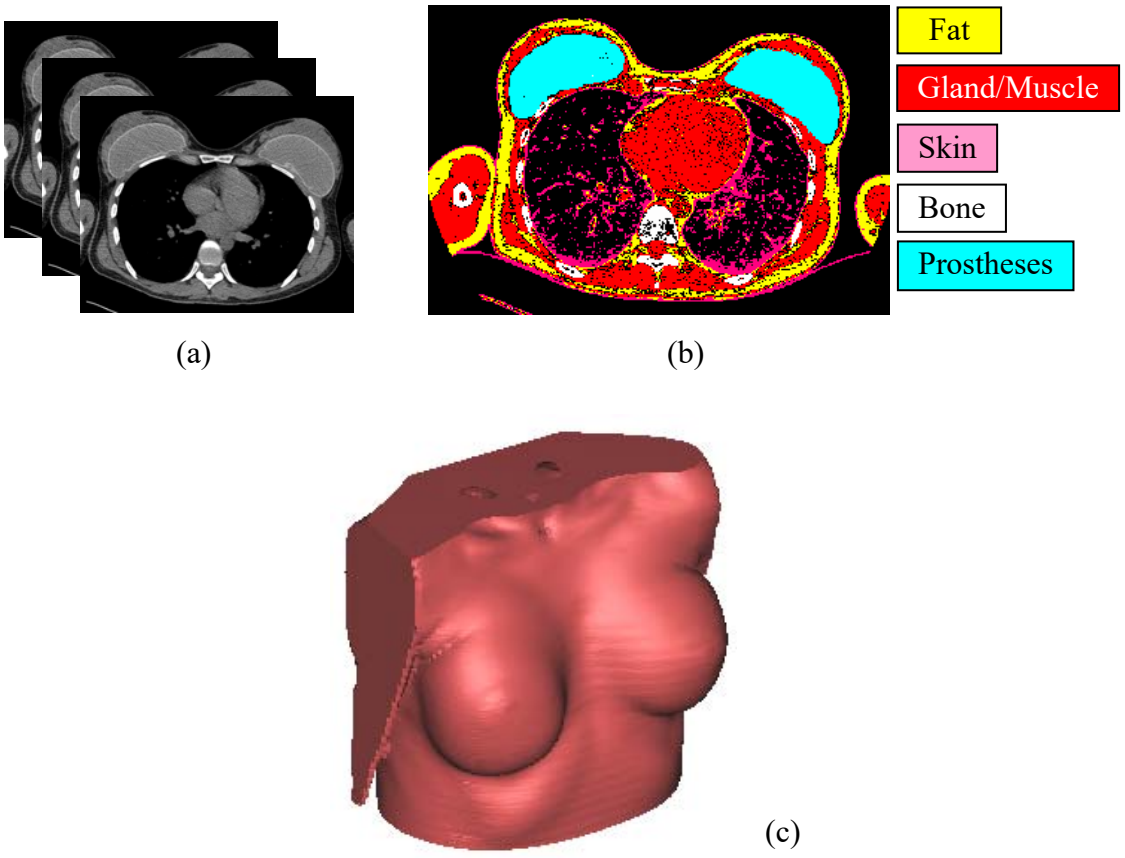

Figure 2. Geometric model of the patient's breast after augmentation mammoplasty to be further compared with the deformed shape of the previously generated FE model. (a) Different CT slices taken after augmentation mammoplasty, where the prostheses can be easily identified. (b) Tissue segmentation on a slice sample. (c) Geometric model of the patient's breast after surgery.

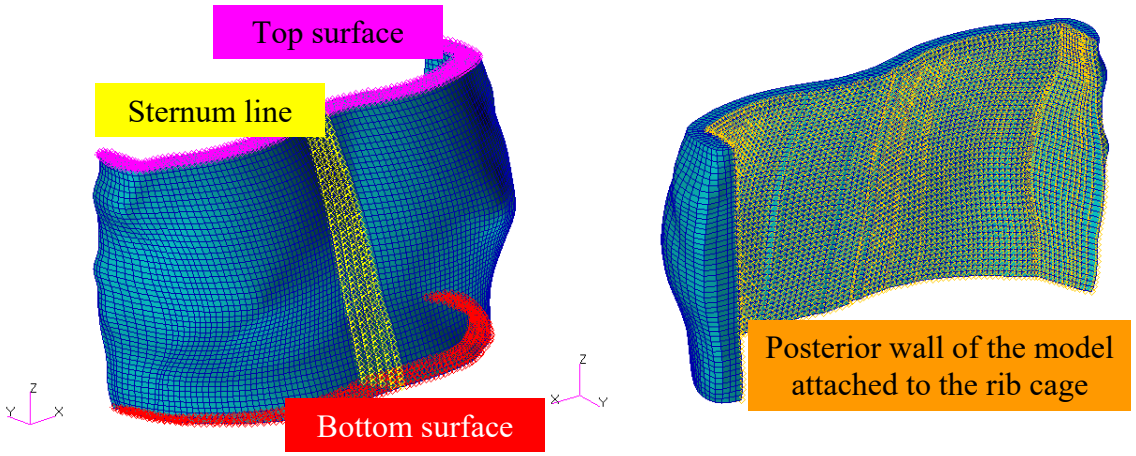

Figure 3. Anteroposterior (left) and posteroanterior (right) views showing color-coded nodes from different anatomical locations where fixed displacement boundary conditions were applied.

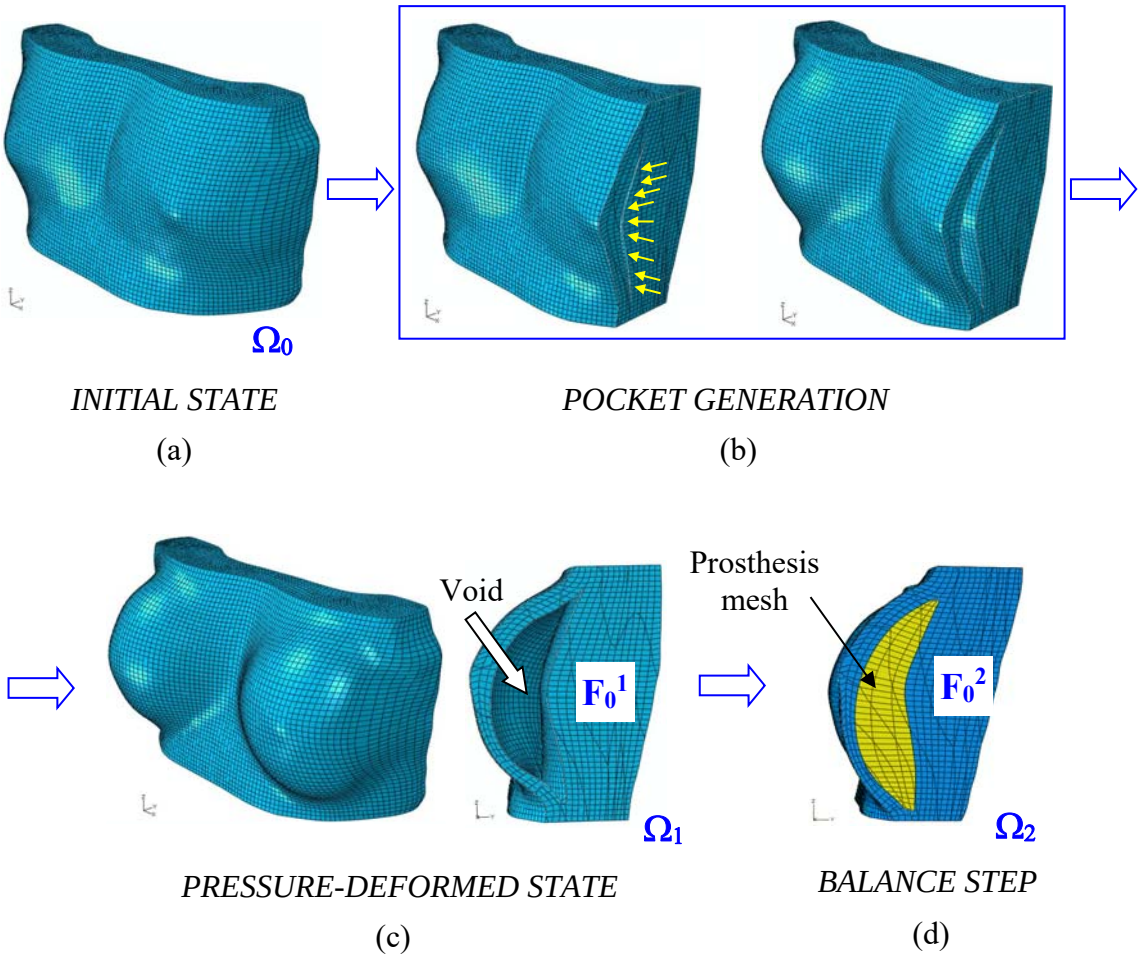

Figure 4. FE simulation scheme of prosthesis insertion. (a) Initial (undeformed) state of the FE model of the patient before surgery. (b) Cut views of the left breast showing two loading stages of the pocket generation. Pressure applied on the loading surface is symbolized by yellow arrows. (c) Perspective and lateral views of the totally deformed breast with residual stresses in the FE elements. Empty space is marked with a white arrow. (d) FE model where meshes representing the silicone prostheses were allocated.

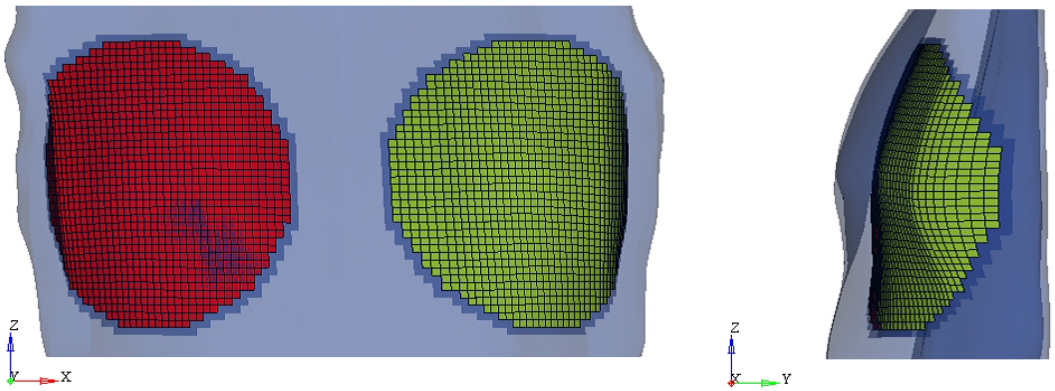

Figure 5. Views sketching the position of the loading surfaces in the FE model (yellow: left breast, red: right breast).

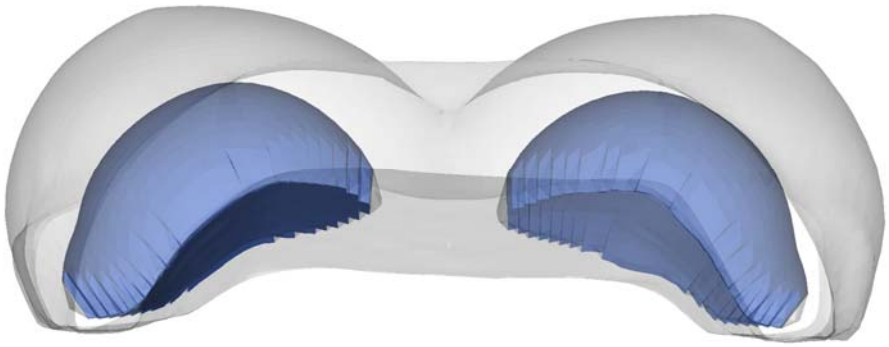

Figure 6. Deformed FE model of the patient lying in supine position, where the meshes of the prostheses are shown in blue.

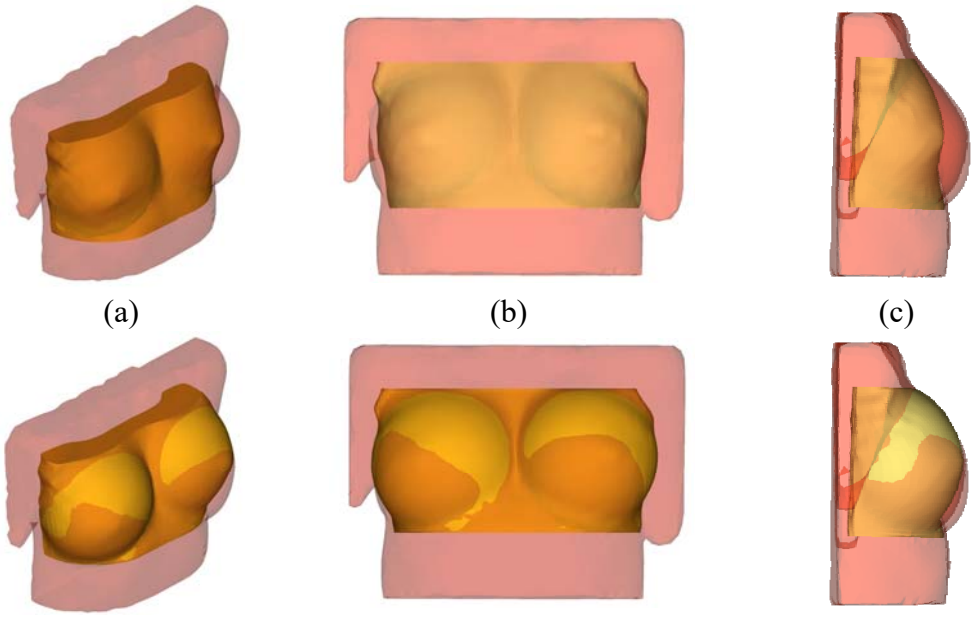

Figure 7. Superposition of the FE model (yellow) with the geometric model of the patient following surgery (red): (a), (b) and (c) before simulation; (d), (e) and (f) after simulation.

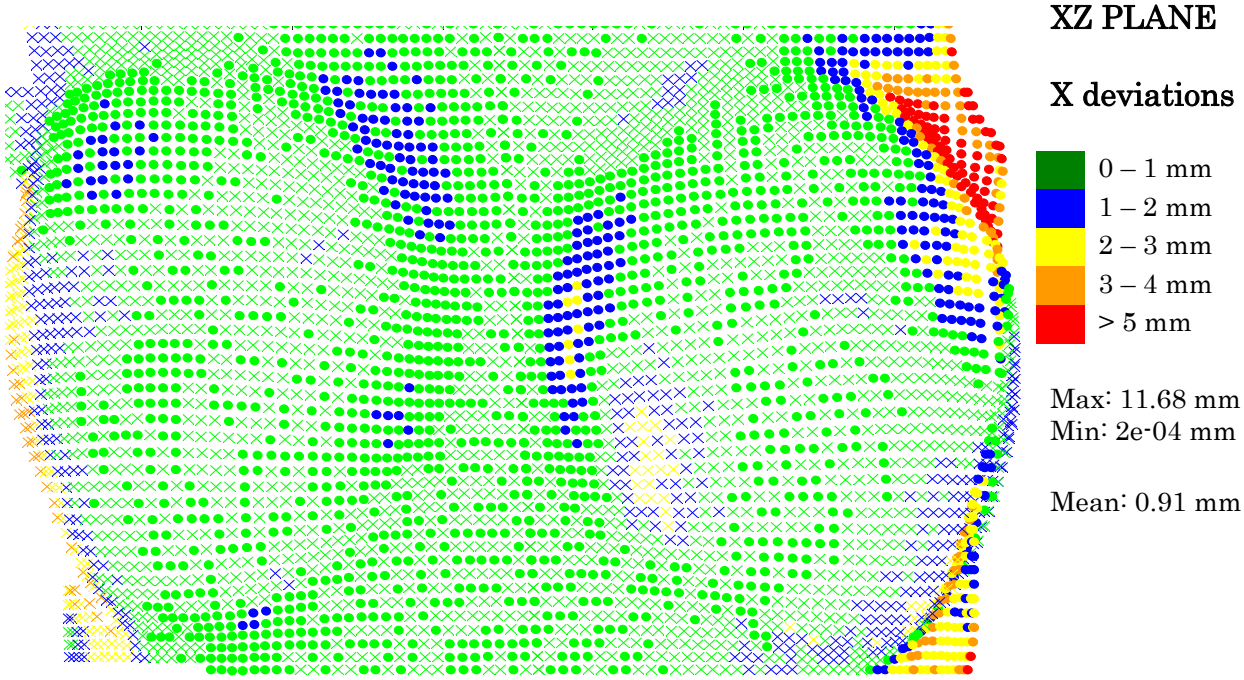
XZ PLANE
X deviations
0 – 1 mm
1 – 2 mm
2 – 3 mm
3 – 4 mm
> 5 mm
Max: 11.68 mm
Min: 2e-04 mm
Mean: 0.91 mm

(a)

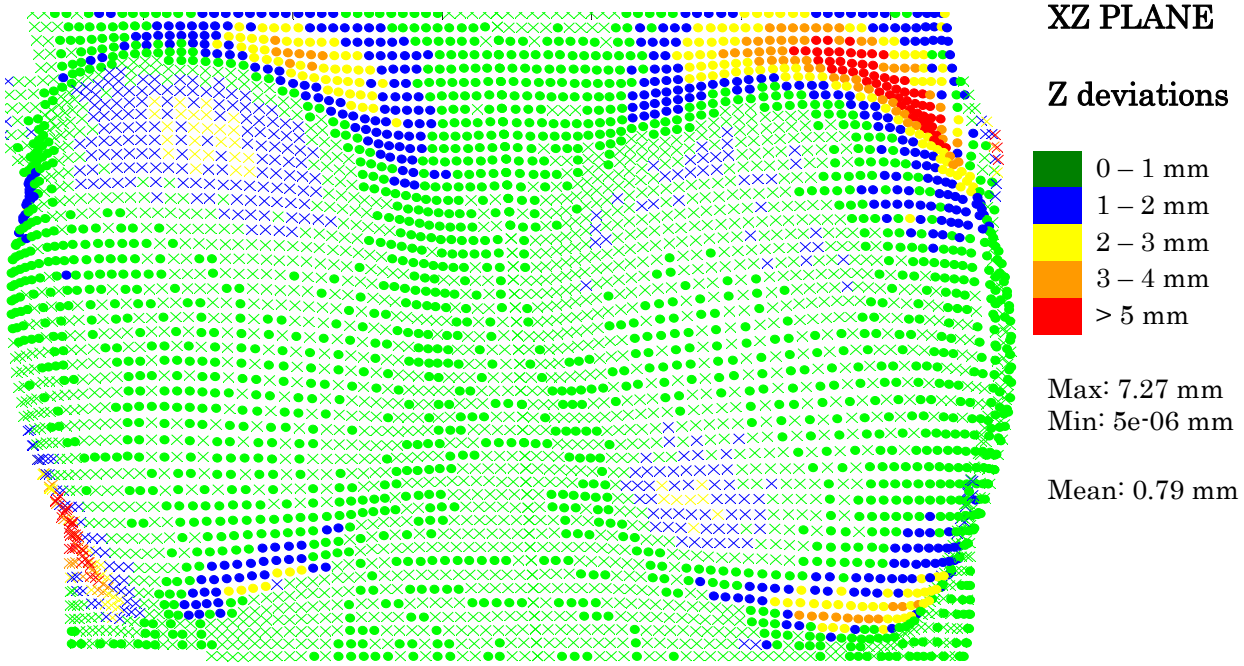
XZ PLANE
Z deviations
0 – 1 mm
1 – 2 mm
2 – 3 mm
3 – 4 mm
> 5 mm
Max: 7.27 mm
Min: 5e-06 mm
Mean: 0.79 mm

(b)

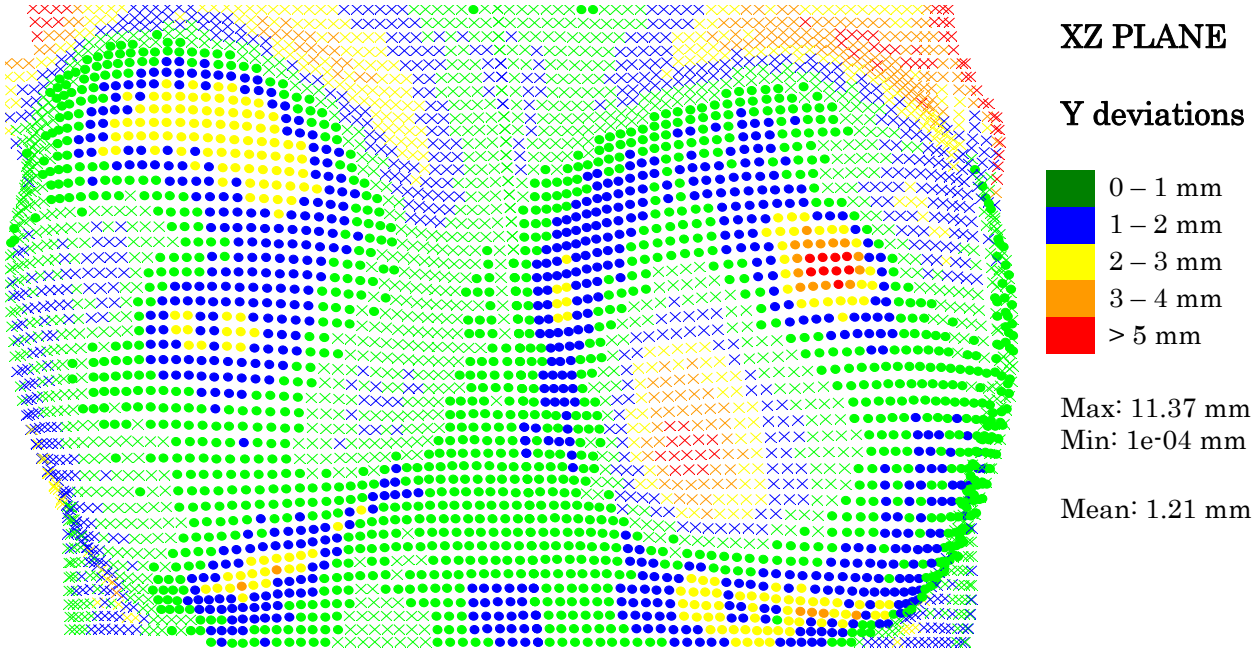

(c)

Figure 8. Color-coded graph distributions showing the deviations of the peripheral nodes of the deformed configuration of the FE model from the geometry of the patient in the frontal plane (XZ). (a) Horizontal deviations ($x_{pat} - x_{FEM}$). (b) Vertical deviations ($z_{pat} - z_{FEM}$). (c) Anteroposterior deviations ($y_{pat} - y_{FEM}$). In all graphs, dots (●) indicate positive deviation while crosses (×) indicate negative deviation. Maximum, minimum and mean values are given in terms of absolute values.

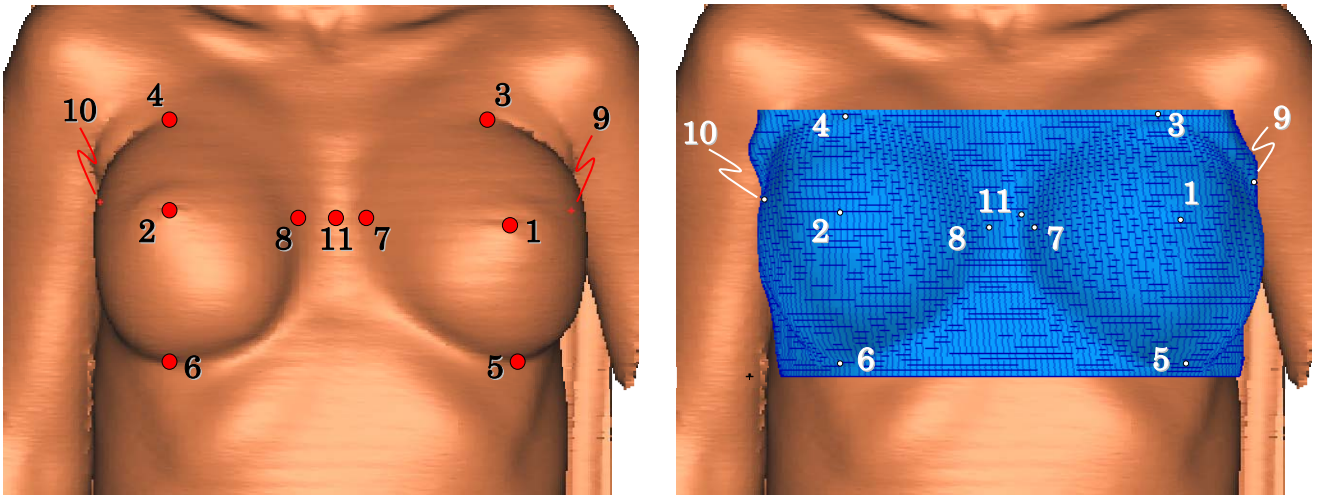

(a) (b)

Figure 9. (a) Nodal markers in the geometric model of the patient lying in supine position after surgery. (b) Nodal markers in the deformed shape of the FE model. (1) Left nipple, (2) right nipple, (3) upper left pole, (4) upper right pole, (5) lower left pole (6) lower right pole, (7) medial left, (8) medial right, (9) axilar left, (10) axilar right and (11) sternum. Nodal markers (9) and (10) are placed beside each breast in this view.